

TERNARY SUPERCONDUCTING HYDRIDES IN THE LA–MG–H SYSTEM

GRIGORIY SHUTOV¹, DMITRII SEMENOK², IVAN KRUGLOV^{3,4}, AND ARTEM OGANOV¹

ABSTRACT. Ternary or more complex hydrogen-rich hydrides are the main hope of reaching room-temperature superconductivity at high pressures. Their chemical space is vast and its exploration is challenging. Here we report the investigation of the La–Mg–H ternary system using the evolutionary algorithm USPEX at pressures on the range 150–300 GPa. Several ternary superconducting hydrides were found, including thermodynamically stable $P6/mmm$ -LaMg₃H₂₈ with $T_C = 164$ K at 200 GPa, $P/2m$ -LaMgH₈, $C2/m$ -La₂MgH₁₂ and $P2/m$ -La₃MgH₁₆. In addition, novel binary hydrides were predicted to be stable at various pressures, such as Cm -Mg₆H₁₁, $P1$ -MgH₂₆, $Fmm2$ -MgH₃₀, $P1$ -MgH₃₈ and $R\bar{3}m$ -LaH₁₃. We also report several novel low-enthalpy metastable phases, both ternary and binary ones. Finally, we demonstrate important methods of exploring very large chemical spaces and show how they can improve crystal structure prediction.

Introduction

The highest-temperature superconductors known today are polyhydrides - hydrides anomalously rich in hydrogen (above what can be expected based on atomic valences). Their studies were anticipated with the hypothesis proposed by Ashcroft [1] that hydrogen-rich materials can become superconductors at high pressures. Some hydride systems demonstrate high superconducting critical temperature, such as $Im\bar{3}m$ -H₃S with $T_C = 203$ K [2], $Fm\bar{3}m$ -LaH₁₀ with $T_C = 250$ K [3, 4], $P6_3/mmc$ -ThH₉ and $Fm\bar{3}m$ -ThH₁₀ with $T_C = 146$ K and $T_C = 159 - 161$ K [5], respectively, and $Im\bar{3}m$ -YH₆ with $T_C = 224 - 226$ K [6].

Semenok et al. [7] showed that high- T_C superconducting hydrides are formed by elements of II-III groups, such as calcium, strontium, barium, scandium, yttrium, lanthanum and lutetium. Elements grouped near these (to a lesser extent near sulfur) in the periodic table often form binary hydrides with the predicted $T_C > 100$ K.

The search for polyhydrides continues in ternary systems. Ternary hydrides $Fm\bar{3}m$ -(La,Y)H₁₀ have been synthesized, and $T_C = 253$ K has been reported [8]. Lithium phosphorus hydride $Pm\bar{3}$ -LiPH₆ has been predicted to be a superconductor with $T_C = 150 - 167$ K [9].

As $T_C = 250$ K of LaH₁₀ has been proven experimentally [3, 4], we can presume that ternary hydrides of lanthanum and some other element may also be high-temperature superconductors. In this work, we study phases formed by lanthanum, magnesium and hydrogen and their superconducting properties.

¹SKOLKOVO INSTITUTE OF SCIENCE AND TECHNOLOGY, MOSCOW, RUSSIA

²CENTER FOR HIGH PRESSURE SCIENCE AND TECHNOLOGY ADVANCED RESEARCH (HPSTAR), BEIJING, CHINA

³MOSCOW INSTITUTE OF PHYSICS AND TECHNOLOGY, MOSCOW, RUSSIA

⁴DUKHOV RESEARCH INSTITUTE OF AUTOMATICS (VNIIA), MOSCOW, RUSSIA

E-mail addresses: Grigoriy.Shutov@skoltech.ru.

Date: December 13, 2023.

Lanthanum hydrides have been theoretically predicted to form several phases at high pressures: $P6/mmm$ -LaH₂, $Cmmm$ -La₃H₁₀, $I4/mmm$ -LaH₄, $Fm\bar{3}m$ -LaH₁₀, and $P6/mmm$ -LaH₁₆ [10]. Moreover, experimental synthesis revealed 7 phases of binary lanthanum hydrides [11]. According to predictions, LaH₁₀ is a superconductor with $T_C = 274$ – 286 K [12]. Magnesium hydrides also form four phases at 200 GPa: $P6_3/mmc$ -MgH₂, $Cmcm$ -MgH₄, $R\bar{3}$ -MgH₁₂, and $P1$ -MgH₁₆. However, they have relatively low reported T_C : 29–37 K for MgH₄ and 20 K for MgH₂ and 47–60 K for MgH₁₂. For MgH₁₆, T_C has not been calculated [13]. Another study reports $Im\bar{3}m$ -MgH₆ with $T_C = 260$ K at pressure above 300 GPa [14].

In this work, we use the evolutionary algorithm USPEX [15, 16, 17] to study the chemical space of the La–Mg–H system. For more detailed search of La–Mg–H ternary hydrides, we additionally perform evolutionary searches on the pseudobinary sections formed by Mg–H and La–H binary hydrides.

Methods

The evolutionary algorithm USPEX [15, 16, 17] was used to predict thermodynamically stable phases. To investigate the La–Mg–H system, we performed both fixed- and variable-composition searches at 200 GPa.

One of the possible straightforward ways to search for new stable hydrides in La–Mg–H system is to perform USPEX calculations in the ternary system. However, such search requires large computational resources, because the chemical space of ternary systems is huge. To tackle this problem, we performed variable-composition searches on special pseudobinary sections of the convex hull with LaH_{*x*}–MgH_{*y*} ($x = 2, 4, 10, 16$, $y = 2, 4, 12, 16$) composition blocks. In addition, we performed variable-composition searches with such composition blocks as LaH_{*x*}–Mg and La–MgH_{*y*} ($x = 2, 4, 10, 16$, $y = 2, 4, 12, 16$ as well). The parameters of each search are presented in Supplementary Materials, Table S1.

After studying the pseudobinary sections, the ternary variable-composition search at 200 GPa pressure was performed, using previously found structures as seeds. The number of generations was 100. After this search, several ternary hydrides remained on the convex hull. Moreover, novel binary hydrides were discovered. Using stable and metastable structures at pressure of 200 GPa as seeds, ternary convex hulls were also calculated at 150, 250 and 300 GPa. Additionally, we recalculated these ternary convex hulls on the temperature range from 0 K to 2000 K, using free energies computed by Phonopy. Metastable structures with the energy above hull $E_{\text{Hull}} \leq 10$ meV/atom are also presented on each convex hull in this work.

Structure relaxations and energy estimation were performed using the VASP code [18, 19, 20] within density functional theory (DFT) [21, 22], implementing the Perdew–Burke–Ernzerhof (PBE) exchange–correlation functional [23] and the projector-augmented wave (PAW) method [24, 25]. The kinetic energy cutoff was set at 600 eV. Γ -centered k -point meshes with a resolution of $2\pi \times 0.05 \text{ \AA}^{-1}$ were used for sampling the Brillouin zone.

The phonon band structure and density of states were computed using Phonopy [26] package implementing the finite displacement method. $2 \times 2 \times 2$ supercells were generated. The energy cutoff and k -spacing parameters for the VASP calculations were set at 500 eV and $2\pi \times 0.1 \text{ \AA}^{-1}$, respectively. Sumo package [27] was used to visualize the phonon density of states and band structure. The k -points for phonon band structures were chosen using Hinuma’s recommendation [28]. The Phonopy package was also used to calculate zero-point energy (ZPE) corrections and thermal properties, such as the entropy and free energy. In addition, structures’ symmetries were also investigated by the Phonopy package. Some of the predicted structures can be symmetrized to various space groups depending on the tolerance parameter. We chose the maximum symmetry space groups within whose structures exhibited dynamical stability.

To calculate phonon frequencies and electron–phonon coupling (EPC) coefficients, we used Quantum Espresso (QE) package [29] utilizing density functional perturbation theory (DFPT) [30], plane-wave pseudopotential method, and the PZ-HGH [31, 32] pseudopotentials. The q -meshes for each structure were $3 \times 3 \times 3$, except MgH_{26} , MgH_{30} and MgH_{38} , for which it was set to $2 \times 2 \times 2$. The Allen–Dynes [33] formula was used to calculate T_C :

$$(1) \quad T_C = \omega_{\log} \frac{f_1 f_2}{1.2} \exp \left[\frac{-1.04(1 + \lambda)}{\lambda - \mu^* - 0.62\lambda\mu^*} \right].$$

The McMillan formula has the term $f_1 f_2 = 1$, whereas in the Allen–Dynes formula, it is expressed as:

$$(2) \quad f_1 f_2 = \sqrt[3]{1 + \left[\frac{\lambda}{2.46(1 + 3.8\mu^*)} \right]^{3/2}} \cdot \left[1 - \frac{\lambda^2(1 - \omega_2/\omega_{\log})}{\lambda^2 + 3.312(1 + 6.3\mu^*)^2} \right],$$

where μ^* is the Coulomb pseudopotential, with the values in the commonly accepted range from 0.10 to 0.15; λ , ω_2 , and ω_{\log} are the EPC constant, mean square frequency, and logarithmic average frequency, respectively, defined as:

$$(3) \quad \lambda = \int_0^{\omega_{\max}} \frac{2\alpha^2 F(\omega)}{\omega} d\omega,$$

$$(4) \quad \omega_{\log} = \exp \left[\frac{2}{\lambda} \int_0^{\omega_{\max}} \frac{d\omega}{\omega} \alpha^2 F(\omega) \log(\omega) \right],$$

$$(5) \quad \omega_2 = \sqrt{\frac{1}{\lambda} \int_0^{\omega_{\max}} \left[\frac{2\alpha^2 F(\omega)}{\omega} \right] \omega^2 d\omega}.$$

where $\alpha^2 F(\omega)$ is an Eliashberg function.

Moreover, full solution of Eliashberg equations [34] was computed using Allen’s algorithm [35]. This algorithm was implemented in our code published on GitHub [36].

To estimate the thermodynamic properties such as critical magnetic field H_C , superconducting gap $\Delta(0)$ and specific heat jump $\Delta C(T_c)$, we used the semiempirical formulas [37]:

$$(6) \quad \frac{\gamma T_C^2}{H_C^2(0)} = 0.168 \left[1 - 12.2 \left(\frac{T_C}{\omega_{\log}} \right)^2 \ln \left(\frac{\omega_{\log}}{3T_C} \right) \right],$$

$$(7) \quad \frac{2\Delta(0)}{k_B T_C} = 3.53 \left[1 + 12.5 \left(\frac{T_C}{\omega_{\log}} \right)^2 \ln \left(\frac{\omega_{\log}}{2T_C} \right) \right],$$

$$(8) \quad \frac{\Delta C(T_c)}{\gamma T_c} = 1.43 \left[1 + 53 \left[\frac{T_c}{\omega_{\log}} \right]^2 \ln \left[\frac{\omega_{\log}}{3T_c} \right] \right],$$

where k_B is the Boltzmann constant and $\gamma = \frac{2}{3}\pi^2 k_B^2 N(0)(1 + \lambda)$ is the Sommerfeld constant. The values of T_C from the solution of Eliashberg equations were used in these formulas.

We note that lower and upper critical magnetic fields H_{C1} and H_{C2} are related to H_C by the following equation:

$$(9) \quad H_C = \frac{\sqrt{H_{C1}H_{C2}}}{\sqrt{\ln \kappa}}$$

where κ is Ginzburg-Landau parameter, and that H_{C2} is usually one or two orders of magnitude higher than H_C . For example, $\kappa = 20$, $H_{C1} = 0.55$ T and $H_{C2} = 143.5$ T were reported for $Fm\bar{3}m$ -LaH₁₀ [38], leading to $H_C = 5.13$ T. Formula (6) returns $H_C = 6.7$ T, which is close to the experimental value.

Ternary convex hulls and phase diagrams, recalculated with ZPE correction on $P = 150, 200, 250$ and 300 GPa, are presented in Figure 1. They revealed $P/2m$ -LaMgH₈, $C2/m$ -La₂MgH₁₂ and $P6/mmm$ -LaMg₃H₂₈ that are stable at $P = 200, 250$ and 300 GPa and $P2/m$ -La₃MgH₁₆ that is stable at $P = 150$ GPa.

Additionally, ternary variable-composition search at 200 GPa revealed novel binary lanthanum and magnesium hydrides: $R\bar{3}m$ -LaH₁₃, $C2/m$ -LaH₂₃, Cm -Mg₆H₁₁, $P1$ -MgH₂₆, $Fmm2$ -MgH₃₀ and $P1$ -MgH₃₈.

Convex hulls and phase diagrams at non-zero temperatures are presented in Supplementary materials (see Figure S1-S4). Crystal structures are presented in Table S2.

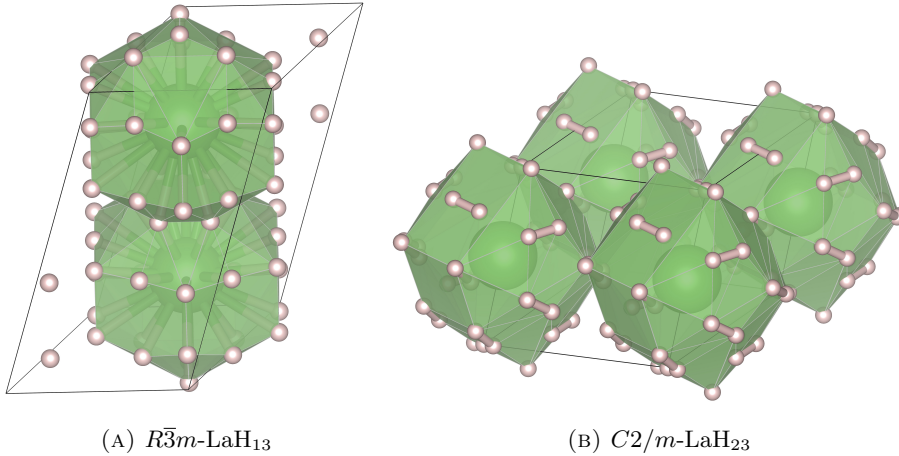


FIGURE 2. Crystal structures of novel lanthanum binary hydrides (visualized by VESTA software [39])

Novel binary hydrides Novel binary lanthanum hydride $R\bar{3}m$ -LaH₁₃ (see Figure 2a) is thermodynamically stable at the pressures 200 GPa and 250 GPa. At 250 GPa, its H-H distances are 0.90 Å while its average La-H distance is 2.02 Å. As demonstrated in Table 1, novel lanthanum hydride has T_C higher than 100 K. It is interesting to note that this phase can shed light on the solution of the long-standing problem of the LaH₁₂ structure, found experimentally, but not yet theoretically explained [40].

Another novel lanthanum hydride $C2/m$ -LaH₂₃ (see Figure 2b) is metastable by 6.8 meV/atom at $P = 150$ GPa. It contains H₂ molecules with H-H distances from 0.77 Å to 0.89 Å. Its average La-H distance is 2.12 Å. At $P = 150$ GPa it has $T_C = 85.1$ K. At $P = 200$ GPa its T_C increases up to 100.5 K, however, its E_{Hull} also increases to 12 meV/atom.

Like previously reported [13] $R\bar{3}m$ -MgH₁₂ and $P\bar{1}$ -MgH₁₆, novel magnesium hydrides $P1$ -MgH₂₆, $Fmm2$ -MgH₃₀ and $P1$ -MgH₃₈ contain molecular hydrogen. As demonstrated in Figure 3 (a-c), their unit cells contain separate H₂ molecules. Moreover, Mg atoms are surrounded by belts of 6 H₂ molecules, similarly to MgH₁₂ and MgH₁₆. Average H-H distances are 0.77 Å, 0.77 Å and 0.76 Å for MgH₂₆, MgH₃₀ and MgH₃₈, respectively. Mean Mg-H distances are 1.74 Å, 1.74 Å and 1.75 Å for MgH₂₆, MgH₃₀ and MgH₃₈, respectively. All novel magnesium hydrides have similar structures (see Figure 3) and similar parameters of their superconducting state, including low T_C s (see Table 1). These molecular magnesium hydrides are similar to

TABLE 1. Superconducting parameters of novel binary hydrides

Parameter	LaH ₁₃	LaH ₁₃	LaH ₁₃	LaH ₂₃	LaH ₂₃
	200 GPa	250 GPa	300 GPa	150 GPa	200 GPa
λ	1.42	1.69	1.60	0.97	1.11
ω_{\log} , K	906	812	1105	1195	1059
ω_2 , K	1454	1505	1669	1819	1844
T_C (McM), K	98	103	134	79	86
T_C (A-D), K	118	137	164	87	99
T_C (E), K	131	155	172	85	101
N_f , $\frac{\text{states}}{\text{Ry}\cdot\text{\AA}^3}$	0.091	0.097	0.101	0.091	0.096
γ , $\frac{\text{mJ}}{\text{cm}^3\cdot\text{K}^2}$	0.126	0.150	0.152	0.103	0.116
$\frac{\Delta C}{T_C}$, $\frac{\text{mJ}}{\text{cm}^3\cdot\text{K}^2}$	0.347	0.445	0.430	0.208	0.265
$\Delta(0)$, meV	26.4	34.0	35.6	14.5	18.2
$\frac{2\Delta(0)}{k_B T_C}$	4.67	5.08	4.78	3.97	4.19
$H_C(0)$, T	1.7	2.2	2.6	1.0	1.1
Electron transfer, e per H atom	0.231	0.231	0.231	0.130	0.130

Parameter	Mg ₆ H ₁₁	MgH ₂₆	MgH ₃₀	MgH ₃₈
	200 GPa	200 GPa	200 GPa	200 GPa
λ	0.53	0.55	0.59	0.51
ω_{\log} , K	898	1282	979	1002
ω_2 , K	1332	2273	2179	2167
T_C (McM), K	14	22	22	13
T_C (A-D), K	14	23	23	14
T_C (E), K	14	23	20	12
N_f , $\frac{\text{states}}{\text{Ry}\cdot\text{\AA}^3}$	0.058	0.071	0.064	0.054
γ , $\frac{\text{mJ}}{\text{cm}^3\cdot\text{K}^2}$	0.051	0.063	0.059	0.047
$\frac{\Delta C}{T_C}$, $\frac{\text{mJ}}{\text{cm}^3\cdot\text{K}^2}$	0.076	0.095	0.090	0.069
$\Delta(0)$, meV	2.2	3.5	3.2	1.8
$\frac{2\Delta(0)}{k_B T_C}$	3.57	3.58	3.59	3.55
$H_C(0)$, T	0.1	0.2	0.2	0.1
Electron transfer, e per H atom	1.091*	0.077	0.067	0.053

T_C was calculated using McMillan (McM), Allen-Dynes (A-D) formulas, and numerical solution of Eliashberg equations (E) with Coulomb pseudopotential $\mu^* = 0.1$.

*one hydrogen atom can accept not more than one electron. Numbers greater than 1 indicate the presence of bonds between metal atoms.

the previously discovered polyhydrides of strontium SrH₂₂ [41], barium BaH₁₂ [42], cesium CsH₁₅₋₁₇ [43], and rubidium RbH₁₉ [44].

Ternary La-Mg-H hydrides Using ternary convex hulls, recalculated with zero-point energy correction, we found two novel ternary hydrides (Figure 1): $C2/m$ -La₂MgH₁₂ at pressures 150 GPa, 200 GPa and 250 GPa and $P6/mmm$ -LaMg₃H₂₈ at 200 GPa and 250 GPa. In

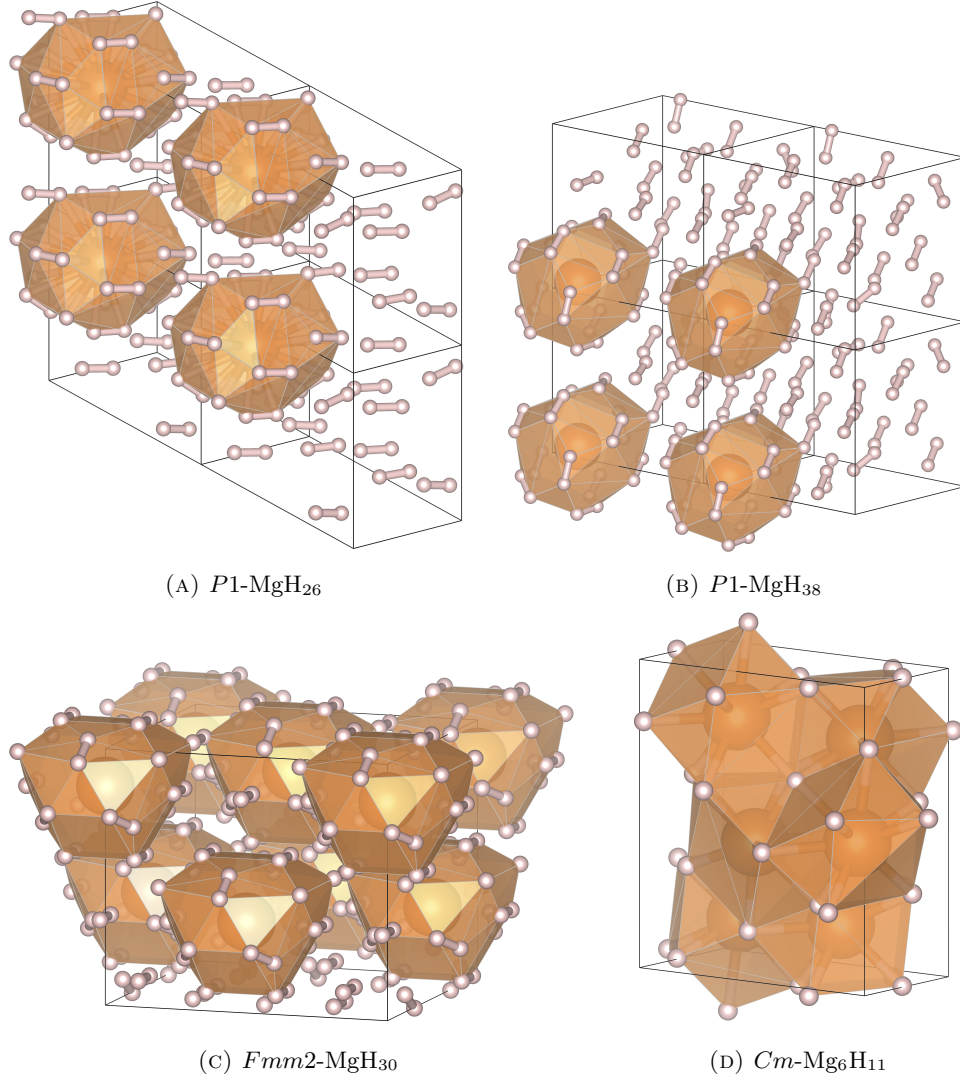


FIGURE 3. Crystal structures of novel magnesium binary hydrides

$\text{LaMg}_2\text{H}_{12}$, La and Mg have coordination numbers 20 and 15, respectively. $\text{LaMg}_3\text{H}_{28}$ has La and Mg coordination numbers 30 and 20, respectively (see Figure 5). In comparison to $C2/m\text{-La}_2\text{MgH}_{12}$, it is hydrogen-rich and has high symmetry.

LaMgH_8 , $\text{La}_2\text{MgH}_{12}$ and $\text{La}_3\text{MgH}_{16}$ lie at the same pseudobinary section of the convex hull: $\text{LaH}_4\text{-MgH}_4$ (see FIG 1). LaMgH_8 , $\text{La}_2\text{MgH}_{12}$ are thermodynamically stable at pressures 200 GPa, 250 GPa and 300 GPa. At pressure of 150 GPa, they become metastable while $\text{La}_3\text{MgH}_{16}$ becomes stable. As it is demonstrated on Figure 5, they share same La-H and Mg-H polyhedras. In addition to such similarity, their EPC constants λ have close values and vary from $\lambda = 0.60$ to $\lambda = 0.77$ (see Table 2). Their T_C s also have close values: from $T_C = 24$ K to $T_C = 55$ K.

TABLE 2. Superconducting parameters of ternary La-Mg-H hydrides

Parameter	LaMgH ₈	LaMgH ₈	LaMgH ₈	La ₂ MgH ₁₂	La ₂ MgH ₁₂	La ₂ MgH ₁₂
	200 GPa	250 GPa	300 GPa	200 GPa	250 GPa	300 GPa
λ	0.74	0.70	0.67	0.60	0.62	0.68
ω_{\log} , K	1014	1195	1277	1042	1172	1014
ω_2 , K	1642	1778	1866	1744	1927	1889
T_C (McM), K	41	42	40	24	29	33
T_C (A-D), K	44	44	42	25	31	35
T_C (E), K	43	45	38	24	30	32
N_f , $\frac{\text{states}}{\text{Ry}\cdot\text{\AA}^3}$	0.115	0.104	0.096	0.111	0.114	0.142
γ , $\frac{\text{mJ}}{\text{cm}^3\cdot\text{K}^2}$	0.116	0.102	0.092	0.102	0.106	0.137
$\frac{\Delta C}{T_C}$, $\frac{\text{mJ}}{\text{cm}^3\cdot\text{K}^2}$	0.198	0.169	0.146	0.157	0.165	0.220
$\Delta(0)$, meV	6.8	7.1	5.9	3.7	4.6	5.0
$\frac{2\Delta(0)}{k_B T_C}$	3.72	3.69	3.64	3.60	3.61	3.65
$H_C(0)$, T	0.5	0.5	0.4	0.3	0.3	0.4
Electron transfer, e per H atom	0.625	0.625	0.625	0.667	0.667	0.667

Parameter	La ₃ MgH ₁₆	LaMg ₃ H ₂₈	LaMg ₃ H ₂₈	LaMg ₃ H ₂₈
	150 GPa	200 GPa	250 GPa	250 GPa
λ	0.76	1.27	1.15	1.09
ω_{\log} , K	1214	1397	1511	1583
ω_2 , K	1660	1760	1961	2079
T_C (McM), K	51	134	128	124
T_C (A-D), K	54	149	141	136
T_C (E), K	55	164	157	138
N_f , $\frac{\text{states}}{\text{Ry}\cdot\text{\AA}^3}$	0.138	0.102	0.116	0.126
γ , $\frac{\text{mJ}}{\text{cm}^3\cdot\text{K}^2}$	0.139	0.133	0.144	0.151
$\frac{\Delta C}{T_C}$, $\frac{\text{mJ}}{\text{cm}^3\cdot\text{K}^2}$	0.243	0.335	0.342	0.332
$\Delta(0)$, meV	8.9	31.3	28.9	24.4
$\frac{2\Delta(0)}{k_B T_C}$	3.75	4.41	4.28	4.11
$H_C(0)$, T	0.7	2.3	2.2	2.0
Electron transfer, e per H atom	0.688	0.321	0.321	0.321

T_C was calculated using McMillan (McM), Allen-Dynes (A-D) formulas, and numerical solution of Eliashberg equations (E) with Coulomb pseudopotential $\mu^* = 0.1$.

Structure of LaMg₃H₂₈ has higher symmetry and higher La and Mg coordination numbers. Superconducting critical temperature of LaMg₃H₂₈ is the highest in the whole La-Mg-H system studied and is equal to $T_C = 164$ K at 200 GPa and $T_C = 157$ K at 250 GPa. Its Eliashberg function is presented in Figure 4.

Superconducting properties of the hydrides in La-Mg-H system can be explained by electron transfer per hydrogen atom. Its values are demonstrated in Table 1 and Table 2. If the transfer is low (0-0.13e per H atom), then hydrogen atoms form H-H molecules and one observes

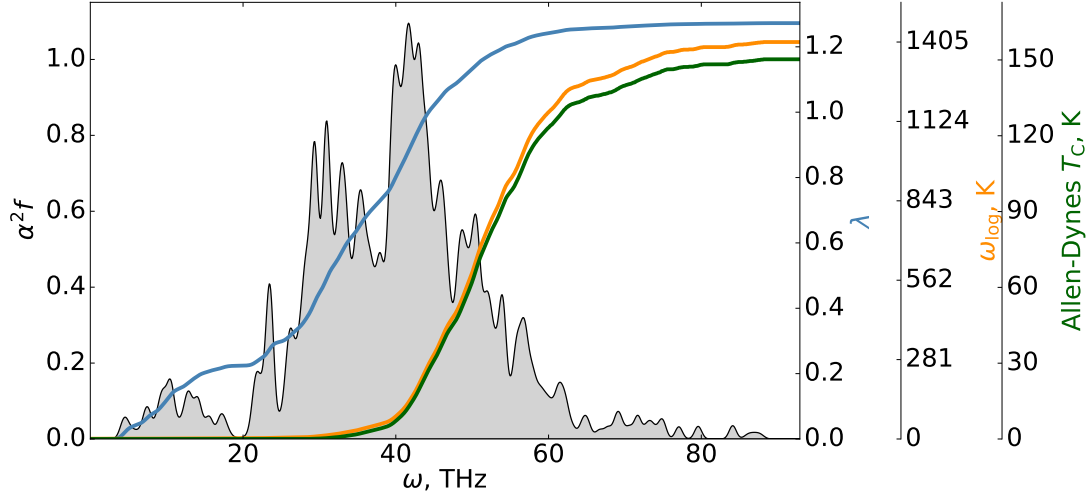


FIGURE 4. Eliashberg function, EPC constant λ , logarithmic average frequency ω_{\log} and critical transition temperature of $\text{LaMg}_3\text{H}_{28}$ at 200 GPa

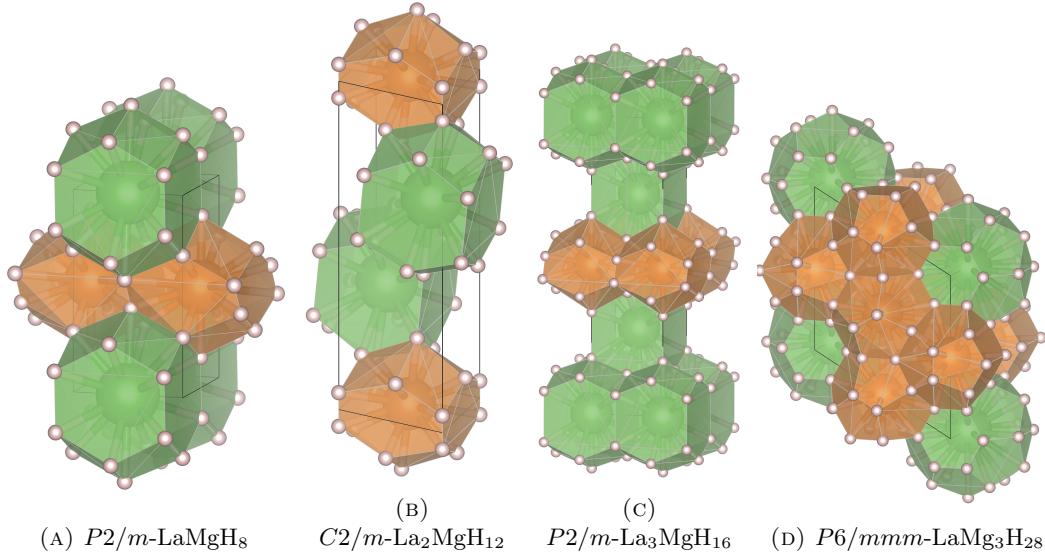


FIGURE 5. Crystal structures of ternary La-Mg-H hydrides

molecular hydrides. Indeed, this is what happens in MgH_{26} , MgH_{30} , MgH_{38} and LaH_{23} . They have lower T_C in comparison to other hydrides with higher transfer. If electron transfer is high ($\approx 1e$ per H atom), then hydrogen atoms become hydride ions H^- and one obtains ionic hydrides or subhydrides with no superconductivity, as it is observed in Mg_6H_{11} . It has been shown [45] that high T_C values correspond to intermediate values of electron transfer around $0.33e$ per H atom. This is confirmed in the La-Mg-H system. $\text{LaMg}_3\text{H}_{28}$ is the hydride with the highest T_C

in the system and it has the transfer of 0.321e per H atom. Other ternary La-Mg-H hydrides with transfer of $\approx 0.6-0.7e$ per H atom have significantly lower T_C .

Conclusions

We have found several novel lanthanum and magnesium binary hydrides which are thermodynamically stable at 150, 200, 250 and 300 GPa. Novel binary $R\bar{3}m$ -LaH₁₃ have T_C s above 100 K. Novel binary $P1$ -MgH₂₆, $Fmm2$ -MgH₃₀ and $P1$ -MgH₃₈ have T_C s below 22 K and crystal structures which are very similar to previously reported [13] $R\bar{3}$ -MgH₁₂ and $P\bar{1}$ -MgH₁₆. T_C s of most ternary La-Mg-H hydrides are below 100 K. However, superconducting critical temperature of $P6/mmm$ -LaMg₃H₂₈ is 164.4 K at 200 GPa, which makes this novel ternary hydride a high-temperature superconductor.

We also demonstrate that variable-composition searches in pseudobinary sections play a crucial role in the exploration of complex chemical spaces. Indeed, most of discovered thermodynamically stable ternary hydrides were initially found on pseudobinary convex hulls. Such searches improve ternary diagrams while being less computationally expensive, so we propose them as an important and useful method in any ternary system exploration.

Acknowledgements

A.O. thanks Russian Science Foundation (grant 19-72-30043) for support of superconducting properties calculations, I.K. thanks Russian Science Foundation (grant 21-73-10261) for support of USPEX search of novel La-Mg-H superconducting hydrides.

References

- [1] N. Ashcroft, Metallic hydrogen: A high-temperature superconductor?, *Phys. Rev. Lett.* 21 (1968) 1748–1749. doi:10.1103/PhysRevLett.21.1748.
- [2] A. Drozdov, M. Eremets, I. Troyan, V. Ksenofontov, S. Shylin, Conventional superconductivity at 203 kelvin at high pressures in the sulfur hydride system, *Nature* 525 (2015) 73–76. doi:10.1038/nature14964.
- [3] A. Drozdov, P. Kong, V. Minkov, S. Besedin, M. Kuzovnikov, S. Mozaffari, L. Balicas, F. Balakirev, D. Graf, V. Prakapenka, E. Greenberg, D. Knyazev, M. Tkacz, M. Eremets, Superconductivity at 250 K in lanthanum hydride under high pressures, *Nature* 569 (2019) 528–531. doi:10.1038/s41586-019-1201-8.
- [4] M. Somayazulu, M. Ahart, A. Mishra, Z. Geballe, M. Baldini, Y. Meng, V. Struzhkin, R. Hemley, Evidence for Superconductivity above 260 K in Lanthanum Superhydride at Megabar Pressures, *Physical Review Letters* 122 (2019) 27001. doi:10.1103/PhysRevLett.122.027001.
- [5] A. Kvashnin, D. Semenov, I. Kruglov, I. Wrona, A. Oganov, High-temperature superconductivity in a th-h system under pressure conditions, *ACS applied materials & interfaces* 10 (2018) 43809–43816. doi:10.1021/acsami.8b17100.
- [6] I. Troyan, D. Semenov, A. Kvashnin, A. Sadakov, O. Sobolevskiy, V. Pudalov, A. Ivanova, V. Prakapenka, E. Greenberg, A. Gavriluk, I. Lyubutin, V. Struzhkin, A. Bergara, I. Errea, R. Bianco, M. Calandra, F. Mauri, L. Monacelli, R. Akashi, A. Oganov, Anomalous high-temperature superconductivity in yh₆, *Advanced Materials* 33 (2021) 2006832. doi:10.1002/adma.202006832.
- [7] D. Semenov, I. Kruglov, I. Savkin, A. Kvashnin, A. Oganov, On Distribution of Superconductivity in Metal Hydrides, *Current Opinion in Solid State and Materials Science* 24 (2020) 100808. doi:10.1016/j.cossms.2020.100808.
- [8] D. Semenov, I. Troyan, A. Ivanova, A. Kvashnin, I. Kruglov, M. Hanfland, A. Sadakov, O. Sobolevskiy, K. Pervakov, I. Lyubutin, K. Glazyrin, N. Giordano, D. Karimov, A. Vasiliev, R. Akashi, V. Pudalov, A. Oganov, Superconductivity at 253 k in lanthanum-yttrium ternary hydrides, *Materials Today* 48 (2021) 18–28. doi:10.1016/j.mattod.2021.03.025.
- [9] Z. Shao, D. Duan, Y. Ma, H. Yu, H. Song, H. Xie, D. Li, F. Tian, B. Liu, T. Cui, Ternary superconducting phosphorus hydrides stabilized via lithium, *npj Computational Materials* 5 (2019) 1–8. doi:10.1038/s41524-019-0244-6.
- [10] I. Kruglov, D. Semenov, H. Song, R. 's, I. Wrona, R. Akashi, M. Davari, D. Duan, T. Cui, A. Kvashnin, A. Oganov, Superconductivity of lah₁₀ and lah₁₆ polyhydrides, *Phys. Rev. B* 101 (2020) 024508. doi:10.1103/PhysRevB.101.024508.
- [11] D. Laniel, F. Trybel, B. Winkler, F. Knoop, T. Fedotenko, S. Khandarkhaeva, A. Aslandukova, T. Meier, S. Chariton, K. Glazyrin, et al., High-pressure synthesis of seven lanthanum hydrides with a significant variability of hydrogen content, *Nature Communications* 13 (2022) 6987. doi:10.1038/s41467-022-34755-y.
- [12] H. Liu, I. Naumov, R. Hoffmann, N. Ashcroft, R. Hemley, Potential high-*t_c* superconducting lanthanum and yttrium hydrides at high pressure, *Proceedings of the National Academy of Sciences* 114 (2017) 6990–6995. doi:10.1073/pnas.1704505114.
- [13] D. Lonie, J. Hooper, B. Altintas, E. Zurek, Metallization of magnesium polyhydrides under pressure, *Physical Review B - Condensed Matter and Materials Physics* 87 (2013) 1–8. doi:10.1103/PhysRevB.87.054107.
- [14] X. Feng, J. Zhang, G. Gao, H. Liu, H. Wang, Compressed sodalite-like mgh₆ as a potential high-temperature superconductor, *RSC Adv.* 5 (2015) 59292–59296. doi:10.1039/C5RA11459D.
- [15] A. Oganov, C. Glass, Crystal structure prediction using ab initio evolutionary techniques: Principles and applications, *Journal of Chemical Physics* 124 (2006).
- [16] A. Oganov, A. Lyakhov, M. Valle, How evolutionary crystal structure prediction works-and why, *Accounts of Chemical Research* 44 (2011) 227–237. doi:10.1021/ar1001318.
- [17] A. Lyakhov, A. Oganov, H. Stokes, Q. Zhu, New developments in evolutionary structure prediction algorithm USPEX, *Computer Physics Communications* 184 (2013) 1172–1182. doi:10.1016/j.cpc.2012.12.009.
- [18] G. Kresse, J. Furthmüller, Efficient iterative schemes for ab initio total-energy calculations using a plane-wave basis set, *Phys. Rev. B* 54 (1996) 11169–11186. doi:10.1103/PhysRevB.54.11169.
- [19] G. Kresse, Ab initio molecular dynamics for liquid metals, *Journal of Non-Crystalline Solids* 192-193 (1995) 222 – 229. doi:10.1016/0022-3093(95)00355-X.
- [20] G. Kresse, J. Hafner, Ab initio molecular-dynamics simulation of the liquid-metal-amorphous-semiconductor transition in germanium, *Phys. Rev. B* 49 (1994) 14251–14269. doi:10.1103/PhysRevB.49.14251.

- [21] P. Hohenberg, W. Kohn, Inhomogeneous electron gas, *Phys. Rev.* 136 (1964) B864–B871. doi:10.1103/PhysRev.136.B864.
- [22] W. Kohn, L. Sham, Self-consistent equations including exchange and correlation effects, *Phys. Rev.* 140 (1965) A1133–A1138. doi:10.1103/PhysRev.140.A1133.
- [23] J. Perdew, K. Burke, M. Ernzerhof, Generalized gradient approximation made simple, *Phys. Rev. Lett.* 77 (1996) 3865–3868. doi:10.1103/PhysRevLett.77.3865.
- [24] P. Blöchl, Projector augmented-wave method, *Phys. Rev. B* 50 (1994) 17953–17979. doi:10.1103/PhysRevB.50.17953.
- [25] G. Kresse, D. Joubert, From ultrasoft pseudopotentials to the projector augmented-wave method, *Phys. Rev. B* 59 (1999) 1758–1775. doi:10.1103/PhysRevB.59.1758.
- [26] A. Togo, I. Tanaka, First principles phonon calculations in materials science, *Scripta Materialia* 108 (2015) 1–5. doi:10.1016/j.scriptamat.2015.07.021.
- [27] A. Ganose, A. Jackson, D. Scanlon, Sumo: Command-line tools for plotting and analysis of periodic ab initio calculations, *Journal of Open Source Software* 3 (2018) 717. doi:10.21105/joss.00717.
- [28] Y. Hinuma, G. Pizzi, Y. Kumagai, F. Oba, I. Tanaka, Band structure diagram paths based on crystallography, *Computational Materials Science* 128 (2017) 140–184. doi:10.1016/j.commatsci.2016.10.015.
- [29] P. Giannozzi, S. Baroni, N. Bonini, M. Calandra, R. Car, C. Cavazzoni, D. Ceresoli, G. Chiarotti, M. Cococcioni, I. Dabo, A. Corso, S. Gironcoli, S. Fabris, G. Fratesi, R. Gebauer, U. Gerstmann, C. Gougoussis, A. Kokalj, M. Lazzeri, L. Martin-Samos, N. Marzari, F. Mauri, R. Mazzarello, S. Paolini, A. Pasquarello, L. Paulatto, C. Sbraccia, S. Scandolo, G. Sclauzero, A. Seitsonen, A. Smogunov, P. Umari, R. Wentzcovitch, QUANTUM ESPRESSO: a modular and open-source software project for quantum simulations of materials, *Journal of Physics: Condensed Matter* 21 (2009) 395502. doi:10.1088/0953-8984/21/39/395502.
- [30] S. Baroni, S. Gironcoli, A. Dal, P. Giannozzi, Phonons and related crystal properties from density-functional perturbation theory, *Rev. Mod. Phys.* 73 (2001) 515–562. doi:10.1103/RevModPhys.73.515.
- [31] J. Perdew, A. Zunger, Self-interaction correction to density-functional approximations for many-electron systems, *Phys. Rev. B* 23 (1981) 5048–5079. doi:10.1103/PhysRevB.23.5048.
- [32] C. Hartwigsen, S. Goedecker, J. Hutter, Relativistic separable dual-space gaussian pseudopotentials from h to rn, *Phys. Rev. B* 58 (1998) 3641–3662. doi:10.1103/PhysRevB.58.3641.
- [33] P. Allen, R. Dynes, Transition temperature of d-f-band superconductors, *Physical Review B* 8 (1973) 1079–1087. doi:10.1103/PhysRevB.8.1079.
- [34] G. Eliashberg, Interactions between electrons and lattice vibrations in a normal metal, *Journal of Experimental and Theoretical Physics* 34 (1960) 996–1001.
- [35] P. Allen, R. Dynes, Transition temperature of strong-coupled superconductors reanalyzed, *Phys. Rev. B* 12 (1975) 905–922. doi:10.1103/PhysRevB.12.905.
- [36] GitGreg228, A2f.
URL <https://github.com/GitGreg228/a2f>
- [37] J. Carbotte, Properties of boson-exchange superconductors, *Rev. Mod. Phys.* 62 (1990) 1027–1157. doi:10.1103/RevModPhys.62.1027.
- [38] V. Minkov, S. Bud'ko, F. Balakirev, V. Prakapenka, S. Chariton, R. Husband, H. Liermann, M. Eremets, Magnetic field screening in hydrogen-rich high-temperature superconductors, *Nature Communications* 13 (2022) 3194. doi:10.1038/s41467-022-30782-x.
- [39] K. Momma, F. Izumi, Vesta 3 for three-dimensional visualization of crystal, volumetric and morphology data, *Journal of applied crystallography* 44 (2011) 1272–1276. doi:10.1107/S0021889811038970.
- [40] M. Kuzovnikov, *V(p)* equations of state of novel lanthanum and yttrium superhydrides, ELBRUS, 2021.
- [41] D. Semenok, W. Chen, X. Huang, D. Zhou, I. Kruglov, A. Mazitov, M. Galasso, C. Tantardini, X. Gonze, A. Kvashnin, et al., Sr-doped superionic hydrogen glass: Synthesis and properties of srh22, *Advanced Materials* 34 (2022) 2200924. doi:10.1002/adma.202200924.
- [42] W. Chen, D. Semenok, A. Kvashnin, X. Huang, I. Kruglov, M. Galasso, H. Song, D. Duan, A. Goncharov, V. Prakapenka, et al., Synthesis of molecular metallic barium superhydride: pseudocubic bah12, *Nature communications* 12 (2021) 273. doi:10.1038/s41467-020-20103-5.
- [43] D. Semenok, Synthesis, x-ray diffraction and nuclear magnetic resonance studies of cesium and rubidium polyhydrides, 6th International Conference on Matter and Radiation at Extremes, Zhuhai, Guangdong, China, 2023.
- [44] M. Kuzovnikov, Synthesis of novel rubidium superhydrides under high pressure, The Joint 28th AIRAPT and 60th EHPRG International Conference on High Pressure Science and Technology, Edinburgh, UK, 2023.

- [45] F. Peng, Y. Sun, C. Pickard, R. Needs, Q. Wu, Y. Ma, Hydrogen clathrate structures in rare earth hydrides at high pressures: Possible route to room-temperature superconductivity, *Phys. Rev. Lett.* 119 (2017) 107001. doi:10.1103/PhysRevLett.119.107001.